

# ZnO and ZnO-nanorods thin films as supported catalysts for enhanced dye degradation

C. Valero-Luna<sup>a</sup>, M.R. Alfaro Cruz<sup>b,\*</sup>, A. Bañuelos-Frias<sup>a</sup>, and G. Ortega-Zarzosa<sup>c</sup>

<sup>a</sup>Universidad Autónoma de Zacatecas, Unidad Académica de Ingeniería Eléctrica, Ramón López Velarde 801, Zacatecas, Zacatecas 98000, México.

<sup>b</sup>CONAHCYT, Universidad Autónoma de Nuevo León, Facultad de Ingeniería Civil, Av. Universidad s/n. Anáhuac, San Nicolas de los Garza 66450, México.

\*e-mail: malfaroc@uanl.edu.mx; mralfaro@conacyt.mx

<sup>c</sup>Facultad de Ciencias, Universidad Autónoma de San Luis Potosí, Av. Parque Chapultepec 1570, 78210. San Luis Potosí, México.

Received 10 January 2023; accepted 8 May 2024

Zinc oxide (ZnO) thin films and ZnO nanorod thin films were prepared via sol-gel and chemical bath deposition methods at low temperatures, respectively, and tested for their ability to photocatalytically degrade Methylene Blue. Both films were oriented in the c-axis in the (002) plane, but the crystallinity of the ZnO nanorod film was better than the ZnO seed layer. The surface morphology of the ZnO film was in ripple form, allowing the ZnO-nanorods to grow around the ripples and increase the contact area with the solution. The ZnO nanorod film enhances the adsorption process. After 2.49 hours of irradiation, 50% of the dye degrades, and 80% degrades after 6 hours. The structural properties, such as good crystallinity and the orientation in the (002) plane, help improve the films' photocatalytic efficiency. ZnO and ZnO-nanorod films could be considered efficient and green options for the photocatalytic process of decomposing organic pollutants in an aqueous medium.

**Keywords:** Thin films; ZnO; photocatalysis; nanorods; semiconductors.

DOI: <https://doi.org/10.31349/RevMexFis.71.041003>

## 1. Introduction

ZnO is a material with a wide variety of uses and applications. It belongs to the TCO family and has been used in solar cells, gas sensors, photovoltaic devices, ultraviolet light-emitting devices, and photocatalysis [1-7]. ZnO has interesting photocatalytic properties since, despite not having the appropriate band gap (3.3 eV) to absorb visible light, its polar nature in the (002) plane allows him to absorb O<sub>2</sub> and OH<sup>-</sup> ions which produce radicals with high oxidizing power. The OH<sup>-</sup> ions production in an aqueous medium is due to the H<sub>2</sub>O oxidation by photogenerated h<sup>+</sup> during the irradiation, which enhances dye degradation [8-11]. The efficiency of ZnO in optoelectronic, photocatalysis, antimicrobial activity, etc., also depends on the physicochemical properties of ZnO, such as structure size, shape, and morphology [12]. If it centers on morphology, ZnO has the advantage that depending on the deposition method; it can grow in different morphologies, such as flowers, ribbons, nanorods, nanowires, etc. [9]. The one-dimension (1D) morphologies as nanorods, nanotubes, nanowires, etc., are very attractive because this kind of morphology increases the aspect ratio and the high surface-to-volume ratio, which improves the capacity of the ZnO to absorb light or enhance electron mobility [9,11,13].

On the other hand, in photocatalytic processes, it is common to use powders that allow the area of the irradiated material to be greater, increasing the activity. However, one of the disadvantages of using powders is that it is difficult to recover the photocatalyst after the reaction [14-16]. For that,

the use of films is a new opportunity for escalating the photocatalytic reaction and making the photocatalyst easier to use. In this sense, ZnO thin films can be obtained for different methods like atomic layer deposition, chemical bath deposition, pulsed laser deposition, spray pyrolysis, etc. [17-21]. However, one of the most used methods for obtaining ZnO films is sol-gel, in which we can obtain homogeneous films over any substrate through a hydrolysis and condensation reaction. It has been reported that thin films obtained by the sol-gel method have good structural, optical, and electrical properties [22-25], and can be used for photocatalytic applications [26-28]. In the case of ZnO nanorods, chemical bath deposition is a good option for growing 1D structures due to its easy-to-grow films of different semiconductors at low temperatures over different substrates.

In this work, ZnO thin films are obtained by the sol-gel method. ZnO films were used as substrates to grow ZnO nanorods by chemical bath deposition. The thin films were characterized by different techniques to know their optical, structural, and morphological properties. The photocatalytic efficiency of ZnO films was tested in Methylene Blue (MB) degradation.

## 2. Experimental

### 2.1. ZnO thin films

ZnO thin films are obtained by the sol-gel method [29] at room temperature using zinc acetate dehydrate [Fermont,

( $\text{CH}_3\text{COO}$ ) $2\text{Zn}\cdot 2\text{H}_2\text{O}$ ], 2-Methoxyethanol (99%, Sigma-Aldrich,  $\text{CH}_3\text{OCH}_2\text{CH}_2\text{OH}$ ) and MEA [Ethanolamine ACS reagent  $\geq 99.0\%$ , Sigma-Aldrich,  $\text{H}_2\text{N-OH}$ ]. 2-Methoxyethanol and MEA were stirred at  $60^\circ\text{C}$ , and zinc acetate was dissolved inside this solution under constant stirring for 120 minutes. The pH of the solution was 7, and the viscosity of the solution was registered at 6 cp. The aging time was 6 hours at room temperature. We used glass substrates by VWR  $3'' \times 1'' \times 1$  mm; these slides were cleaned in an ultrasonic bath with a mixture of acetone, isopropyl alcohol, and deionized water for 10 minutes and next dried with air. Then the ZnO solution was deposited by dip coating at a constant speed (9 mm/min). Preheating at  $160^\circ\text{C}$  per 10 minutes was done to evaporate solvents and inorganics compounds among each layer. Finally, thin films were annealed in a tubular furnace at  $400^\circ\text{C}$  for 2 hours.

## 2.2. Growth of ZnO nanorods

ZnO thin films obtained by Sol-Gel were used as substrates to grow ZnO nanorods by chemical bath deposition [30]. Zinc nitrate hexahydrate 0.005 M and NaOH 0.26 M were separately dissolved in deionized water, mixed in a beaker (pH 11), and put in a chemical bath at  $70^\circ\text{C}$  for 60 minutes. After this time, ZnO substrates were rinsed in deionized water and dried with air.

## 2.3. Photocatalytic activity of ZnO thin films and ZnO nanorods thin films

The photocatalytic activity of ZnO thin film samples with different morphology was evaluated by Methylene Blue (MB) degradation in an aqueous solution of 5 ppm. Catalytic thin films have an active area of  $1 \times 1 \text{ cm}^2$ . We used three quartz vials with 3 ml of dye solution for the degradation reaction.

The Quartz vials were then irradiated under UV light of 15 W for 1, 2, 3, 4, 5, and 6 hours and analyzed to determine the residual concentration of MB.

## 2.4. Characterization

Structural properties were analyzed using a grazing angle X-ray diffractometer from the PANalytical EMPYREAN model. Transmittance spectra of the ZnO film were measured using a UV-Visible spectrophotometer (UV-VIS-NIR Cary 5000 spectrophotometer) with a wavelength region from 175 to 3300 nm, taking as reference a Corning Glass substrate No  $1 \frac{1}{2} 22 \times 40$  mm. The photocatalytic activity was determined with a UV-VIS spectrophotometer USB4000 from Ocean Optics. Surface images were obtained with a JEOL JSM 6510 scanning electron microscope.

## 3. Results and discussion

### 3.1. Morphology

Figure 1a), b), and c) shows SEM images for ZnO thin film obtained by the Sol-Gel Method. The surface of these films is not entirely homogeneous because too many agglomerations ranging in size from  $1 \mu\text{m}$  to  $20 \mu\text{m}$  are present in the samples. ZnO solution by Sol-Gel was deposited in drops producing many ripples on the borders. The segregation of the phases could be due to the solvent's low volatility and the vapor pressure, causing poor or rich regions of the solution and yielding the presence of ripples over the surface [31]. Over this irregular surface, ZnO-nanorods were grown [Figs. 1e), 1d), and 1f)], covering the entire surface and even enveloping all ripples. Additionally, to the nanorods, stars were found over the surface, which can be formed by excess precipitates over the surface substrates [Figs. 1d), 1e)].

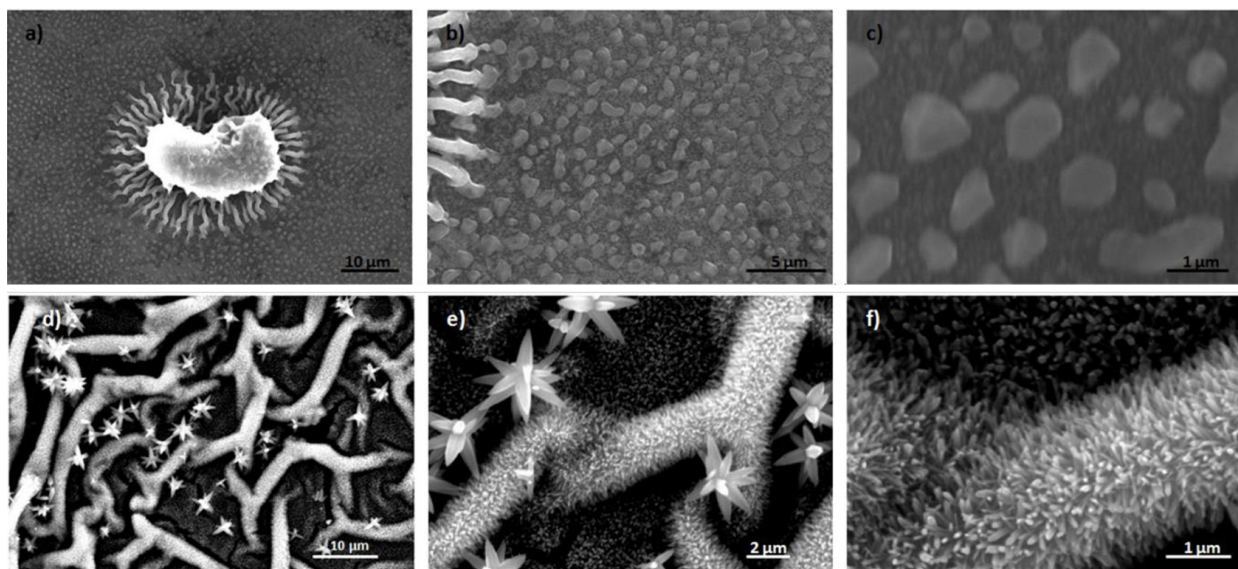


FIGURE 1. SEM images of the surface of the ZnO films a), b), and c) and ZnO nanorods d), e), and f).

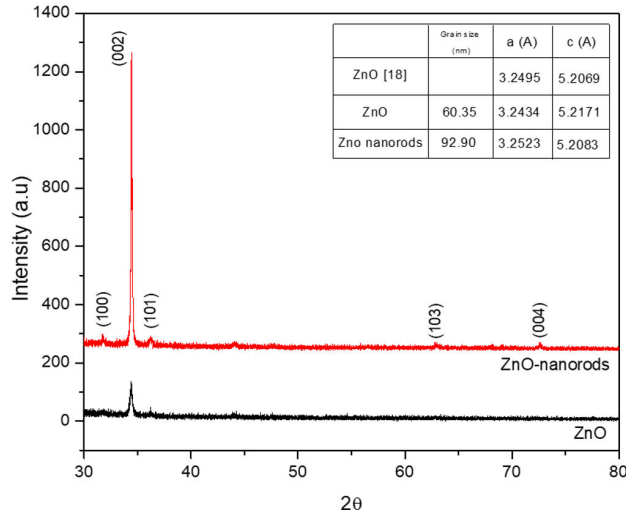


FIGURE 2. XRD diffraction patterns for ZnO and ZnO-nanorods thin films.

### 3.2. XRD

Figure 2 shows XRD diffraction patterns for ZnO and ZnO-nanorods thin films. The peak at  $34.55^\circ$  of the ZnO thin film deposited by Sol-gel has a higher intensity than the other peaks. This peak corresponds to the (002) plane, which means that the film is oriented on the c-axis. As we have seen in SEM results, the ZnO surface has many agglomerates, which could detract from the film's crystallinity. On the other hand, the intensity of the ZnO nanorods increased significantly. Likewise, in the ZnO films, the ZnO nanorods are oriented in the (002) plane since the ZnO film served as the seed layer for the growth of the nanorods. Both films have a hexagonal structure, preferentially oriented on the c-axis (TRACES 6 database, 06-0891 card). Some authors report that preferential orientation is defined by the particle interaction with the substrate [32]; glass substrates are amorphous, so when a solution is deposited over a glass substrate, the growth is random [33].

Therefore, when we grow nanorods over ZnO thin films with a preferential orientation over the c-axis, we force the

solution to grow in this direction and inhibit the growth in other directions. To confirm this, the textural coefficient was calculated by the following equation [34]:

$$T_{c(hkl)} = \frac{I_{(hkl)}}{\frac{1}{n} \sum I_{c(hkl)}}, \quad (1)$$

where,  $I_{(hkl)}$  and  $I_{c(hkl)}$  are the XRD intensities of the experimental data and the standard pattern, and  $n > 1$ , the number of diffraction peaks. As the textured coefficient is for both films, the growth is oriented in a preferential direction  $(h, k, l)$  different from the referent card [35,36], which coincides with those mentioned above. On the other hand, as seen in Fig. 2, the ZnO nanorod film crystallinity is better than the ZnO film, which means that this film has fewer defects than the ZnO film. To confirm this assumption, the dislocation density of each film was calculated using the following equation [37]:

$$\delta = \frac{1}{D^2}, \quad (2)$$

where  $D$  is the grain size. The dislocation density for each film is shown in Table I. It can be observed that the dislocation density is lower for the ZnO nanorods film, which will improve the photocatalytic efficiency [22]. All these kinds of defects, like dislocations, grain boundary, stacking faults, etc., make the films under different sources of strain [38]. Using lattice constant  $c$  values, we can calculate the strain along the  $c$  axis using [39]:

$$\varepsilon = \frac{a_s - a_L}{a_L} \times 100\%, \quad (3)$$

where  $a_s$  as is the lattice parameter of the strained ZnO from the X-ray diffraction data and  $a_L$  is the unstrained lattice parameter of ZnO. If the strain value is positive, the film is under tensile strain, but if the strain value is negative, the film shows a compressive strain [40]. According to the results, the ZnO film has a tensile stress (positive), while ZnO nanorods have a compressive strain (negative). For hexagonal crystals,

TABLE I. Structural properties of the ZnO films.

	Grain size (nm)	$a$ (Å)	$c$ (Å)	Textured coefficient			Density dislocations ( $\text{nm}^{-2}$ )	Strain (%)	Stress (GPa)
				$T_{C(100)}$	$T_{C(002)}$	$T_{C(101)}$			
ZnO (06-0891)		3.2595	5.2069						
ZnO	3.123	3.2434	5.2171	0.57	2.10	0.31	$9.12 \times 10^{-4}$	0.0084	-3.94
ZnO nanorods	50.98	3.2523	5.2083	0.12	2.80	0.06	$3.85 \times 10^{-4}$	-	46.73
								0.1003	

the biaxial stress ( $\sigma$ ) in the plane of the film can be calculated by the relation [41]:

$$\sigma = \left[ 2(C_{13})^2 - \frac{(C_{11} + C_{12})C_{33}}{C_{13}} \right] \varepsilon, \quad (4)$$

for ZnO, the elastic stiffness constants are  $C_{11} = 2.07 \times 10^{11}$  N/m<sup>2</sup>,  $C_{33} = 2.09 \times 10^{11}$  N/m<sup>2</sup>,  $C_{12} = 1.17 \times 10^{11}$  N/m<sup>2</sup>,  $C_{13} = 1.06 \times 10^{11}$  N/m<sup>2</sup> [42], are negative for the ZnO films and positive for the ZnO nanorods (Table I). Usually, the total stress in thin films comprises two components: extrinsic stress and thermal strain. Extrinsic stress is due to the lattice mismatch and the thermal expansion coefficient between the film and the substrate. In contrast, thermal strain is related to the thermal expansion coefficient among ZnO ( $4.75 \times 10^{-6}$  K<sup>-1</sup>) and glass substrate ( $3.25 \times 10^{-6}$  K<sup>-1</sup>) [40,43]. Some authors report that when the thermal expansion coefficient of the film material is larger than the substrate thermal expansion coefficient, the substrate can induce resultant tensile stress over the film material [43].

### 3.3. Optical properties

The optical properties of ZnO thin films were analyzed using UV-VIS spectroscopy (Fig. 3). The final appearance of thin films was opaque, so the average optical transmittance was about 20 and 30%. The absorption edge was found at 379.5 nm for ZnO thin film, whereas the absorption edge was at 385.3 nm for ZnO-nanorods thin film. The optical band gap for each thin film was determined from the  $(\alpha h\nu)^2$  vs.  $h\nu$  plot. The ZnO thin film band gap was 3.22 eV and 3.24 eV for ZnO-nanorods film. ZnO-nanorods increase carrier concentration enabling lower energy states to be filled to increase the optical band gap [44]. This phenomenon is known as the Burstein-Moss effect [45,46].

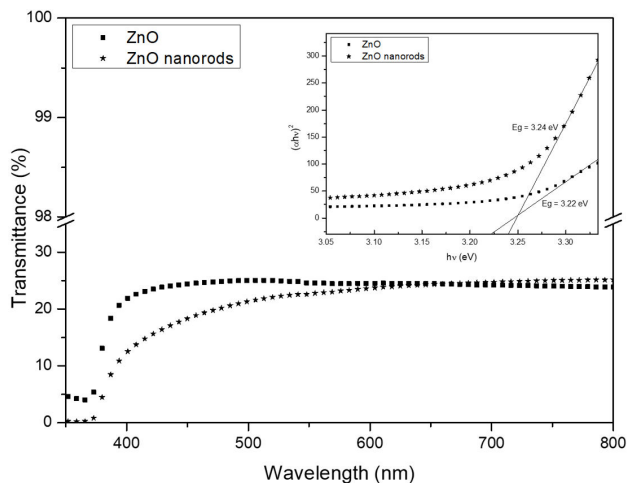


FIGURE 3. Transmittance percentage and optical band gap of ZnO thin films and ZnO nanorods. An increase in the band gap is shown for the thin film of ZnO nanorods.

### 3.4. Photocatalytic degradation of Methylene blue

The degradation of a 5 ppm methylene blue (MB) solution was conducted to probe the photocatalytic activity of ZnO and ZnO-nanorods thin films, as shown in Fig. 4a). First, the adsorption of the MB solution in the dark was carried out for the ZnO ( $\square$ ) and the ZnO-nanorod film ( $\star$ ). Then, to observe that MB degradation was not caused by photolysis, a pure solution of MB was irradiated with UV light ( $\circ$ ). Finally, the MB concentration was plotted vs. time for the ZnO thin films with nanorods ( $\nabla$ ) and without nanorods ( $\square$ ) for a reaction time of 6 hours. The ZnO-nanorods film shows higher photocatalytic activity due to a significant presence of oxygen vacancies that increase surface activity compared to the ZnO film [40,41]. After 6 hours, the MB solution was degraded by around 70% for the ZnO and 80% for the ZnO-nanorods thin films because of the photoreaction [47]. Both thin films have first-order reaction kinetics [Fig. 4b)]. In addition, can be noted a linear relation between  $\ln(C_0/C_t)$  and the irradiation time in the degradation process of the dye [47]. From Fig. 4b), it can be observed that both films have a similar performance in the photocatalytic degradation of methylene blue. Still, the ZnO nanorod's photocatalytic efficiency is better due to high crystallinity, showing a lower presence of defects than the ZnO film (Table I). Also, the advantage of this kind of morphology is that it can improve the effective surface area, allowing better light capture and enhancing the photocatalytic efficiency [48,49]. However, some authors have reported that the photocatalytic efficiency of ZnO is due to the grain size because if a material has a small grain size, this can favor the surface area, giving more sites for better absorption [28].

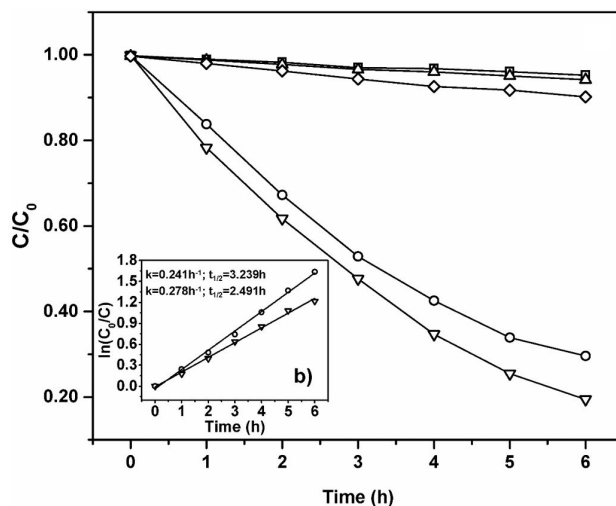


FIGURE 4. a) Evaluation of the MB photocatalytic degradation by the comparison of the initial concentration ( $C_0$ ) and the residual concentration ( $C_t$ ) after different irradiation times and b) the determination of the  $K_{app}$ . The Adsorption of MB on the ZnO ( $\square$ ) and ZnO- nanorods ( $\star$ ) thin films, auto-photodegradation of MB ( $\circ$ ), the photocatalytic activity of the ZnO thin film ( $\square$ ), and the ZnO-nanorod film ( $\star$ ).

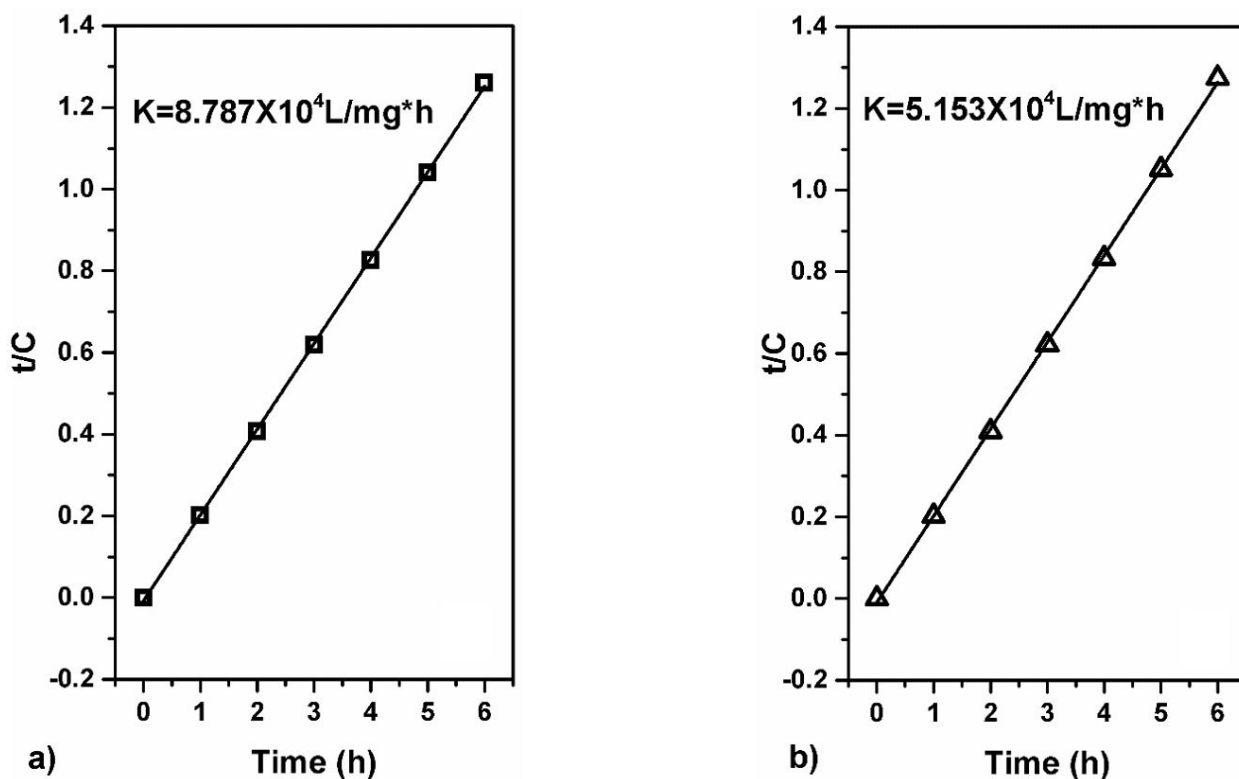


FIGURE 5. Study of the adsorption kinetics of the MB on the surface of the ZnO thin film ( ) and the ZnO-nanorods thin film (□). Both of them showed Langmuir-type behavior.

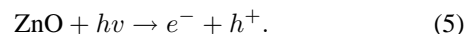
Using this information, it was possible to determine the rate constant  $k$  and the semi-reaction period  $t_{1/2}$ , resulting in  $k = 0.214 \text{ h}^{-1}$  and  $t_{1/2} = 3.293 \text{ h}$  for the Zn films. And  $k = 0.278 \text{ h}^{-1}$  with  $t_{1/2} = 2.491 \text{ h}$  for the ZnO-nanorod films. Reaction kinetics are also highly related to other parameters such as the amount of the catalyst, light intensity, temperature, etc. [47]. The reaction speed rate increases in the presence of the nanorods, which can be attributed mainly to an improvement in surface area, generating an increase in the dye adsorption on the surface of the catalyst. It took about 2.49 hours of irradiation to degrade until 50% of the dye. The structural properties, such as good crystallinity and the orientation in the (002) plane, help to improve the ZnO films' photocatalytic efficiency.

Figure 5 shows the adsorption kinetics of the MB molecules on the surface of the ZnO-nanorods thin film (a) and the ZnO thin film (b). Both showed Langmuir-type behavior, corresponding to the formation of MB monolayers on the catalyst surface. The absorption rate constants were calculated by the linearization of the absorption curves from Fig. 4a). A rise in the adsorption rate for the ZnO-nanorods film ( $8.787/\text{mg} \cdot \text{h}$ ) is noted in comparison to the rate of the ZnO film ( $5.153 \times 10^4 \text{ L/mg} \cdot \text{h}$ ) because of the increase in surface area.

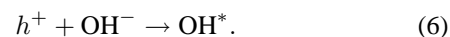
Table II compares the percentage of photodegradation among various catalysts, including suspended and supported  $\text{TiO}_2$ ,  $\text{BaFe}_{12}\text{O}_{19}$ , and ZnO films for the degradation of MB

solution. Therefore, we can state that the presented ZnO and ZnO thin films straightforwardly prepared by the chemical bath deposition method deliver excellent photocatalytic performance for the degradation as they can degrade from 70-80% of the MB solution in 6 hours. It can be noted that depending on the synthesis method, it was produced different particle sizes, morphology, and total surface area. This yields variations in the photocatalytic performance of each catalyst. The ZnO catalyst films presented in this work show better degradation performance than the work of Ali, *et al.*

The proposed reaction mechanism for the rupture of the MB under UV irradiation ( $h\nu = 3.24$  and  $3.22 \text{ eV}$ ) is as follows:



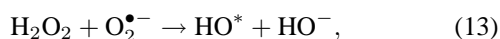
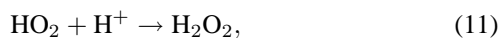
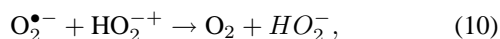
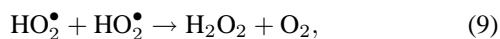
The decomposition of the BM molecule is induced by the high reactivity of the  $h^+$  and the subsequent formation of the hydroxyl radical due to the water decomposition.



Furthermore, electrons on the conduction band surface can produce superoxide ions by reducing molecular  $\text{O}_2$ . Moreover, this radical is known to produce organic peroxides  $\text{H}_2\text{O}_2$  as well. In addition, hydroxyl radical can be generated by capturing photogenerated electrons by the presence of  $\text{O}_2$  dissolved in the reaction mixture.

TABLE II. Comparison of the photocatalytic degradation of MB among various catalyst.

Catalyst	Light source	% MB solution degradation	Irradiation time (hours)	Reference
Ceramic disk supported TiO <sub>2</sub>	UV	64	3	Teekateerawej <i>et al.</i> (2006)
Immobilized TiO <sub>2</sub> on Pyrex	UV	75	4.4	Vaiano <i>et al.</i> (2015)
ZnO and ZnO-nanorods films (Chemical bath deposition)	UV	70, 80	6	This work
ZnO films (magnetron sputtered and hydrothermal deposition)	UV	80	24	Ali <i>et al.</i> (2011)
N-doped TiO <sub>2</sub> immobilized	UV-Visible	100	2	Sacco <i>et al.</i> , (2019)



Finally, it can be addressed that, as proposed in our previous work [54], the photodegradation of MB is produced first by the rupture of the chromophore of the dye molecule, followed by the appearance of organic compounds composed by -CH<sub>3</sub> groups, double bonds, alkane - CH<sub>2</sub>, and ketones. This can be confirmed by the study of Ali, *et al.*, 2011, in which an HPLC analysis found that the photodegradation of MB by ZnO thin films produces four major reaction species Azure B (AB), Azure A (AA), Azure C (AC) and Thionine (TH). In addition, this study demonstrated that the MB molecule was not completely oxidized in the observed reaction time, due to the production of secondary compounds, which generates a decrease in the probability of the interaction between the catalyst and the MB dye molecules [55].

## 4. Conclusions

The ZnO and ZnO-nanorods thin films prepared by the Sol-Gel method demonstrated excellent catalytic activity for the degradation of the MB model molecule. Since it has a greater contact surface that favors the interaction between the methylene blue molecule and the catalyst, it promotes a greater rate of photodegradation of the dye molecule than the ZnO thin film. One of the main advantages of these catalytic thin films is that they are inexpensive and can be straightforwardly fabricated, easily recovered, and reused. In addition, the ZnO catalyst particles do not have to be recovered from the reaction mixture using traditional chemical methods. This makes the presented ZnO and ZnO-nanorod films efficient and green approaches for photocatalytic decomposing organic pollutants in an aqueous medium.

## Acknowledgments

The authors would like to thank Facultad de Ciencias, UASLP, Coordinación para la Innovación y Aplicación de la Ciencia y la Tecnología (CIACYT-UASLP) for the facilities in the characterization of the thin films.

1. R. Kumar *et al.*, Zinc oxide nanostructure-based dye-sensitized solar cells, *J. Mater. Sci.* **52** (2021) 4743, <https://doi.org/10.1007/s10853-016-0668-z>.
2. P. Dhamodharan, J. Chen, and C. Manoharan, Fabrication of dye-sensitized solar cells with ZnO nanorods as photoanode and natural dye extract as sensitizer, *J Mater Sci: Mater Electron* **32** (2021) 13418, <https://doi.org/10.1007/s10854-021-05920-8>.
3. X. Atanacio-Sánchez *et al.*, Improving performance of ZnO flexible dye sensitized solar cell by incorporation of graphene

- oxide, *Microsyst Technol* **26** (2020) 3591, <https://doi.org/10.1007/s00542-020-04820-x>.
- M. Sinha, R. Mahapatra, B. Mondal, and R. Ghosh, A High-Sensitivity Gas Sensor Toward Methanol Using ZnO Microrods: Effect of Operating Temperature, *Journal of Elec Materi* **46** (2017) 2476, <https://doi.org/10.1007/s11664-017-5316-0>.
  - A.B. Khatibani, Investigation of gas sensing property of zinc oxide thin films deposited by Sol-Gel method: effects of molarity and annealing temperature. *Indian J Phys* **95** (2021) 243, <https://doi.org/10.1007/s12648-020-01689-4>.
  - N. Elamin, A. Modwi, M.A.B. Aissa, K. Kamal, Omer K. Taha, and T. A. Al-Duaij, Fabrication of Cr-ZnO photocatalyst by starch-assisted sol-gel method for photodegradation of congo red under visible light, *J Mater Sci: Mater Electron* **32** (2021) 2234, <https://doi.org/10.1007/s10854-020-04988-y>.
  - M.S. Hamdy, *et al.*, Novel Mg@ZnO nanoparticles synthesized by facile one-step combustion route for anti-microbial, cytotoxicity and photocatalysis applications, *J Nanostruct Chem* **11** (2021) 147, <https://doi.org/10.1007/s40097-020-00355-9>.
  - E. Luévano-Hipólito, and L.M. Torres-Martínez, Sonochemical synthesis of ZnO nanoparticles and its use as photocatalyst in H<sub>2</sub> generation, *Mater. Sci. Eng. B* **226** (2017) 223, <https://doi.org/10.1016/j.mseb.2017.09.023>.
  - P. K. Aspoukeh, A. A. Barzinjy, and S.M. Hamad, Synthesis, properties and uses of ZnO nanorods: a mini review, *Int Nano Lett* **12** (2022) 153, <https://doi.org/10.1007/s40089-021-00349-7>.
  - F. Mikailzade *et al.*, Structural, optical, and magnetic characterization of nanorod-shaped polycrystalline Zn<sub>1-x</sub>MnxO films synthesized using sol-gel technique, *Appl. Phys. A* (2020) 126, <https://doi.org/10.1007/s00339-020-03953-0>.
  - S. Goktas, and A. Goktas, A comparative study on recent progress in efficient ZnO based nanocomposite and heterojunction photocatalysts: A review, *J Alloy Compd* **863** (2021) 158734, <https://doi.org/10.1016/j.jallcom.2021.158734>.
  - C. Reddy Chandraiahgari *et al.*, Synthesis and characterization of ZnO nanorods with a narrow size distribution, *RSC Adv* **5** (2015) 49861, <https://doi.org/10.1039/C5RA02631H>.
  - A. Aljaafari, F. Ahmed, C. Awada, and N. M. Shaalan, Flower-Like ZnO Nanorods Synthesized by Microwave-Assisted One-Pot Method for Detecting Reducing Gases: Structural Properties and Sensing Reversibility, *Front. Chem.* **8** (2020) 456, <https://doi.org/10.3389/fchem.2020.00456>.
  - A. Di Mauro, M. Elena Fragalà, V. Privitera, and G. Impellizzeri, ZnO for application in photocatalysis: From thin films to nanostructures, *Mat Sci Semicon Proc* **69** (2017) 44, <https://doi.org/10.1016/j.mssp.2017.03.029>.
  - K. Echendu, S. Z. Werta, F. B. Dejene, and V. Craciun, Electrochemical deposition and characterization of ZnOS thin films for photovoltaic and photocatalysis applications, *J Alloy Compd* **769** (2018) 201, <https://doi.org/10.1016/j.jallcom.2018.07.327>.
  - M. R. Islam, M. Rahman, S. F. U. Farhad, and J. Podder, Structural, optical and photocatalysis properties of sol-gel deposited Al-doped ZnO thin films, *Surf Interfaces* **16** (2019) 120, <https://doi.org/10.1016/j.surfin.2019.05.007>.
  - J. Iqbal, A. Jilani, P.M. Ziaul Hassan, S. Rafique, R. Jafer, and A. A. Alghamdi, ALD grown nanostructured ZnO thin films: Effect of substrate temperature on thickness and energy band gap, *Journal of King Saud University - Science* **28** (2016) 347, <https://doi.org/10.1016/j.jksus.2016.03.001>.
  - J. Ungula, and H. C. Swart, Structural, morphological and optical properties of ZnO nanorods grown on a ZnO:Ga seeded thin film: The role of chemical bath deposition precursor concentration at constant and varying II/VI molar ratios, *Thin Solid Films* **687** (2019) 137483, <https://doi.org/10.1016/j.tsf.2019.137483>.
  - E. H. H. Hasabeldaim, O. M. Ntwaeaborwa, R. E. Kroon, E. Coetsee, and H. C. Swart, Luminescence properties of Eu doped ZnO PLD thin films: The effect of oxygen partial pressure, *Supper Lattice Microst* **139** (2020) 106432, <https://doi.org/10.1016/j.spmi.2020.106432>.
  - P. S. Shewale, S. H. Lee, and Y. S. Yu, Effects of annealing temperature of spin-coated ZnO seed-layer on UV photosensing properties of PLD grown ZnO: Mg thin films, *J Alloy Compd* **774** (2019) 461, <https://doi.org/10.1016/j.jallcom.2018.09.294>.
  - P. Nunes, E. Fortunato, P. Tonello, F. Braz Fernandes, P. Vilarinho, and R. Martins, Effect of different dopant elements on the properties of ZnO thin films, *Vacuum* **64** (2002) 281, [https://doi.org/10.1016/S0042-207X\(01\)00322-0](https://doi.org/10.1016/S0042-207X(01)00322-0).
  - G. Ortiz Rabell, M.R. Alfaro Cruz, and I. Juárez-Ramírez, Hydrogen production of ZnO and ZnO/Ag films by photocatalysis and photoelectrocatalysis, *Mat Sci Semicon Proc*, **134** (2021) 105985, <https://doi.org/10.1016/j.mssp.2021.105985>.
  - M. Popa *et al.*, Highly c-axis oriented ZnO thin film using 1-propanol as solvent in sol-gel synthesis, *Mater Lett* **92** (2013) 267, <https://doi.org/10.1016/j.matlet.2012.10.099>.
  - L. Cui, G.-G. Wang, H.-Y. Zhang, R. Sun, X.-P. Kuang, and J.-C. Han, Effect of film thickness and annealing temperature on the structural and optical properties of ZnO thin films deposited on sapphire (0001) substrates by sol-gel, *Ceram Int* **39** (2013) 3261, <https://doi.org/10.1016/j.ceramint.2012.10.014>.
  - F. Yakuphanoglu, Evaluation of photoresponse in solution-processable ZnO thin film transistor for radiative sensor applications, *Sens. Actuators, A*, **173** (2012) 141, <https://doi.org/10.1016/j.sna.2011.11.019>.
  - A. Kulis-Kapusinska *et al.*, Photocatalytic degradation of methylene blue at nanostructured ZnO thin films. *Nanotechnology*, **34** (2023) 155702,

27. F. Zhang, W. Zhang, X. Luo, G. Feng, and L. Zhao, Electrodeposition of ZnO film with enhanced photocatalytic activity towards methylene blue degradation. *International Journal of Electrochemical Science*, **12** (2017) 3756,
28. W. Vallejo, A. Cantillo, and C. Díaz-Uribe, (Methylene blue photodegradation under visible irradiation on Ag-Doped ZnO thin films. (International Journal of Photoenergy, 2020).
29. M. R. Alfaro Cruz *et al.*, Impact of the annealing atmosphere in the electrical and optical properties of ZnO thin films, *J Sol-Gel Sci Technol* **79** (2016) 184, <https://doi.org/10.1007/s10971-016-4035-y>.
30. M. R. Alfaro Cruz *et al.*, Electrical, optical and structural properties of ZnO nanorods thin films deposited over ZnO substrates, *Mater Lett* **133** (2014) 293, <https://doi.org/10.1016/j.matlet.2014.07.014>.
31. H. Kozuka, Radiative Striations in Spin-Coating Films. In: Klein L., Aparicio M., Jitianu A. (eds) Handbook of Sol-Gel Science and Technology. (Springer, Cham. 2016)
32. L. Hongxia *et al.*, Sol-gel preparation of transparent zinc oxide films with highly preferential crystal orientation, *Vacuum* **77** (2004) 57, <https://doi.org/10.1016/j.vacuum.2004.08.003>.
33. E. Jiménez-González, J. A. Soto Urueta, and R. Suárez-Parra, Optical and Electrical Characteristics of Aluminum-Doped ZnO Thin Films Prepared by Sol Gel Technique, *J Cryst Growth* **192** (1998) 430, [https://doi.org/10.1016/S0022-0248\(98\)00422-9](https://doi.org/10.1016/S0022-0248(98)00422-9).
34. Y. Wang, W. Tang, and L. Zhang, Crystalline Size Effects on Texture Coefficient, Electrical and Optical Properties of Sputter-deposited Ga-doped ZnO Thin Films, *J Mater Sci Technol* **31** (2015) 175, <https://doi.org/10.1016/j.jmst.2014.11.009>.
35. Y. Ozlem Altintas, A. Hanife, and S. Savas, Facile synthesis of cobalt-doped zinc oxide thin films for highly efficient visible light photocatalysts, *Appl Surf Sci* **390** (2016) 111, <https://doi.org/10.1016/j.apsusc.2016.08.069>.
36. R. Dom, H. Gyu Kim and P. H. Borse, Efficient hydrogen generation over (100)-oriented ZnO nanostructured photoanodes under solar light, *Cryst Eng Comm* **16** (2014) 2432, <https://doi.org/10.1039/C3CE42058B>.
37. E.S. Rajalekshmi and A. Moses Ezhil Raj, Effect of substrate temperature on structural and morphological studies by spray pyrolysed ZnO thin films, *Solid State Commun*, **338** (2021) 114479, <https://doi.org/10.1016/j.ssc.2021.114479>.
38. T. Ungár, Characterization of nanocrystalline materials by X-ray line profile analysis, *J Mater Sci*, **42** (2007) 1584, <https://doi.org/10.1007/s10853-006-0696-1>.
39. D. Raoufi and T. Raoufi, The effect of heat treatment on the physical properties of sol-gel derived ZnO thin films, *Appl. Surf. Sci.*, **255** (2009) 5812, <https://doi.org/10.1016/j.apsusc.2009.01.010>.
40. M.F. Malek, Thermal annealing-induced formation of ZnO nanoparticles: Minimum strain and stress ameliorate preferred c-axis orientation and crystal-growth properties, *J Alloy Compd* **610** (2014) 575, <https://doi.org/10.1016/j.jallcom.2014.05.036>.
41. Y. G. Wang *et al.*, Comprehensive study of ZnO films prepared by filtered cathodic vacuum arc at room temperature, *J. Appl. Phys.* **94** (2003) 1597, <https://doi.org/10.1063/1.1592007>.
42. R. Kumar, N. Khare, V. Kumar, and G. L. Bhalla, Effect of intrinsic stress on the optical properties of nanostructured ZnO thin films grown by rf magnetron sputtering, *Appl. Surf. Sci.*, **254** (2008) 6509, <https://doi.org/10.1016/j.apsusc.2008.04.012>.
43. Stephen Beeby, MEMS Mechanical Sensors, Artech House, 2004.
44. O. Tuna, Y. Selamet, G. Aygun, and L. Ozyuzer, High quality ITO thin films grown by dc and RF sputtering without oxygen, *J Phys D Appl Phys* **43** (2010) 055402, <https://doi.org/10.1088/0022-3727/43/5/055402>.
45. Q. Zhu, J. Lu, Y. Wang, Q. Feifei, S. Zengliang, and X. Chunxiang, Burstein-Moss Effect Behind Au Surface Plasmon Enhanced Intrinsic Emission of ZnO, *Microdisks. Sci Rep*, **6** (2016) 36194, <https://doi.org/10.1038/srep36194>.
46. N. Azizah *et al.*, Influence of Al doping on the crystal structure, optical properties, and photodetecting performance of ZnO film, *Pro Nat Sci-Mater* **30** (2020) 28, <https://doi.org/10.1016/j.pnsc.2020.01.006>.
47. R. Mohan, K. Krishnamoorthy, and S. J. Kim, Enhanced photocatalytic activity of Cu-doped ZnO nanorods, *Solid State Commun*, **152** (2012) 375, <https://doi.org/10.1016/j.ssc.2011.12.008>.
48. W. Zhou, H. Lui, R.I. Boughton, G. Du, J. Lin, J. Wang, and D. Lui, One-dimensional single-crystalline Ti-O based nanostructures: properties, synthesis, modifications and applications. *J Mater Chem* **20** (2010) 5993, <https://doi.org/10.1039/B927224K>.
49. X. Wang, Z. Li, J. Shi, and Y. Yu, One-dimensional titanium dioxide nanomaterials: nanowires, nanorods, and nanobelts. *Chem Rev*, **114** (2014) 9346, <https://doi.org/10.1021/cr400633s>.
50. S. Teekateerawej, J. Nishino, and Y. Nosaka, Design and evaluation of photocatalytic micro-channel reactors using TiO<sub>2</sub>-coated porous ceramics, *J Photochem Photobiol. A Chem*, **179** (2005) 263, <https://doi.org/10.1016/j.jphotochem.2005.08.024>.
51. V. Vaiano, O. Sacco, D. Pisano, D. Sannino, and P. Ciambelli, From the design to the development of a continuous fixed bed photoreactor for photocatalytic degradation of organic pollutants in wastewater, *Chem Eng Sci*, **137** (2015) 152, <https://doi.org/10.1016/j.ces.2015.06.023>.
52. A. M. Ali, E. A. C. Emanuelsson, and D. A. Patterson, Conventional versus lattice photocatalysed reactions: Implications of the lattice oxygen participation in the liquid phase photocatalytic oxidation with nanostructured ZnO thin films on reaction products and mechanism at both 254 nm and 340 nm, *Appl Catal B*, **106** (2011) 323, <https://doi.org/10.1016/j.apcatb.2011.05.033>.
53. O. Sacco, D. Sannino, and V. Vaiano, Packed bed photoreactor for the removal of water pollutants using visible light emitting diodes, *Applied Sciences (Switzerland)*, **9** (2019). <https://doi.org/10.3390/app9030472>.

54. C. Valero-Luna, S.A. Palomares-Sánchez, and F. Ruíz, Catalytic activity of the barium hexaferrite with H<sub>2</sub>O<sub>2</sub>/visible light irradiation for degradation of Methylene Blue, *Catal. Today*, **15** (2016) 110, <https://doi.org/10.1016/j.cattod.2015.08.049>.
55. A. M. Ali, E. A.C. Emanuelsson, and D. A. Patterson, Conventional versus lattice photocatalysed reactions: Implications of the lattice oxygen participation in the liquid phase photocatalytic oxidation with nanostructured ZnO thin films on reaction products and mechanism at both 254 nm and 340 nm, *Appl. Catal.*, **106** (2011) 323, <https://doi.org/10.1016/j.apcatb.2011.05.033>.